

## Semiconductor nanostructures via electrodeposition from ionic liquids\*

Rihab Al-Salman<sup>1</sup>, Xiangdong Meng<sup>2,1</sup>, Jiupeng Zhao<sup>3</sup>, Yao Li<sup>2</sup>,  
Ulrich Kynast<sup>4</sup>, Marina M. Lezhnina<sup>4</sup>, and Frank Endres<sup>1,‡</sup>

<sup>1</sup>Institute of Particle Technology, Clausthal University of Technology, D-38678 Clausthal-Zellerfeld, Germany; <sup>2</sup>Center for Composite Materials and Structure, Harbin Institute of Technology, Harbin, 150001, China; <sup>3</sup>School of Chemical Engineering, Harbin Institute of Technology, Harbin, 150001, China; <sup>4</sup>Department of Chemical Engineering, Inorganic Chemistry/Applied Materials Science, University of Applied Sciences, Münster, Germany

**Abstract:** The fascinating properties of ionic liquids make it possible to synthesize semiconductor nanostructures via a simple and low-cost electrochemical pathway. The present paper summarizes our recent work on the synthesis of Si, Ge, and Si<sub>x</sub>Ge<sub>1-x</sub> nanostructures from ionic liquids: thin films, nanowires and photonic crystals. We also introduce our first results on the template-assisted electrodeposition of Si<sub>x</sub>Ge<sub>1-x</sub> photonic crystals from 1-ethyl-3-methylimidazolium bis(trifluoromethylsulfonyl)amide ([EMIm]Tf<sub>2</sub>N) ionic liquid, and some optical measurements on the previously prepared Ge photonic crystals. Our results confirm that electrochemistry in ionic liquids is excellently suited to the synthesis of high-quality semiconductor nanostructures.

**Keywords:** ionic liquids; nanowires; photonic crystals; semiconductor nanostructures; template-assisted electrodeposition; thin films.

### INTRODUCTION

Semiconductor nanostructures stimulated considerable interest as novel materials for future electronic and optoelectronic devices [1,2]. A main fundamental reason behind this is their fascinating electronic and optical properties, which differ from bulk structures and arise at size regimes below 20 nm (according to the material) due to quantum size effects. Besides these interesting properties, Si, Ge, and their alloy Si<sub>x</sub>Ge<sub>1-x</sub> are particularly interesting semiconductors due to their relatively cheap prices. Their nanostructures are currently mainly made by ultra-high-vacuum techniques like molecular beam epitaxy (MBE) and chemical vapor deposition (CVD) [3–8]. In the present paper, we summarize our work on the synthesis of Si, Ge and Si<sub>x</sub>Ge<sub>1-x</sub> thin films, nanowires and 3-dimensionally ordered macroporous (3DOM) nanostructures (photonic crystals) by an electrochemical pathway. Unlike the ultra-high-vacuum techniques, the electrochemical method is relatively simple and comparably cheap. The electrodeposition of the important compound semiconductor CdS, as an example, has recently been shown to be feasible in ionic liquids [9]. As will be presented here, this method has a high potential for the electrodeposition of semiconductors even on the nanometer scale. The Si, Ge, and Si<sub>x</sub>Ge<sub>1-x</sub> nano-

\*Paper based on a presentation on the “Synthesis and Mechanism” theme at the 42<sup>nd</sup> IUPAC Congress, 2–7 August 2009, Glasgow, UK. Other Congress presentations are published in this issue, pp. 1569–1717.

‡Corresponding author: E-mail: frank.endres@tu-clausthal.de

structures are directly obtained via electrodeposition from the following air- and water-stable ionic liquids: 1-butyl-1-methylpyrrolidinium bis(trifluoromethylsulfonyl)amide [ $\text{Py}_{1,4}\text{Tf}_2\text{N}$ ], 1-ethyl-3-methylimidazolium bis(trifluoromethylsulfonyl)amide ( $[\text{EMIm}]\text{Tf}_2\text{N}$ ), and 1-hexyl-3-methylimidazolium tris(pentafluoroethyl)-trifluorophosphate ( $[\text{HMIm}]\text{FAP}$ ), which have significantly wide electrochemical windows [10,11] that allow the deposition of such reactive elements and their alloys without the interference of solvent reduction.  $\text{GeCl}_4$  and/or  $\text{SiCl}_4$  were used as the precursors for semiconductor deposition. The only limitation here is to perform the experiments under inert conditions due to the hygroscopic nature of the precursors. The results showed very clearly that electrochemistry in ionic liquids is pure enough to obtain semiconductors with qualities that are comparable to that from ultra-high-vacuum techniques: The deposited  $\text{Si}_x\text{Ge}_{1-x}$ , as an example, showed different colors ranging from red, blue to green during the electrodeposition due to quantum confinement effects caused by the nanostructure of the deposits. The observed color sequence at room temperature is indicative of a “direct” bandgap behavior of our deposit with a bandgap ranging from at least 1.5 to 3.2 eV [12].

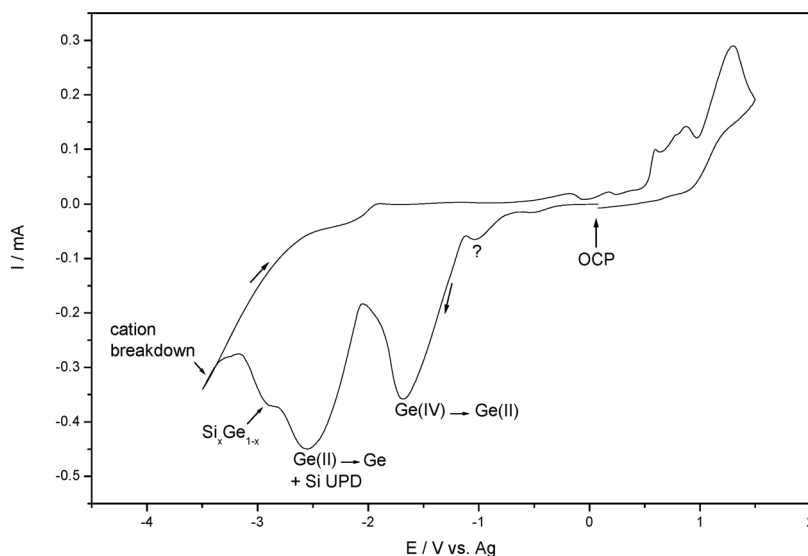
Nanowires of Si, Ge, and their alloy ( $\text{Si}_x\text{Ge}_{1-x}$ ) with diameters of  $\sim 100$  nm have been successfully obtained from  $[\text{Py}_{1,4}\text{Tf}_2\text{N}]$  and  $[\text{EMIm}]\text{Tf}_2\text{N}$  ionic liquids by utilizing track-etched polycarbonate (PC) membranes as templates [13,14]. Moreover, we synthesized 3DOM Ge nanostructures, which are prototypes of a photonic crystal, with air sphere diameters of 370 and 560 nm from ionic liquids by using polystyrene (PS) colloidal crystals as templates [15]. In this paper, we add our first optical measurements of the prepared Ge photonic crystals. We also report herein, for the first time, on the electrodeposition of  $\text{Si}_x\text{Ge}_{1-x}$  photonic crystals from  $[\text{EMIm}]\text{Tf}_2\text{N}$  ionic liquid. PS colloidal crystals with an average diameter of 370 nm were used as templates. In our opinion,  $\text{Si}_x\text{Ge}_{1-x}$  could be an interesting material for photonic crystals, especially if it is prepared in the quantum size regime where a bandgap of up to 3.2 eV can be obtained. In this case, the material would have two important conditions for a photonic crystal that can exhibit a full photonic bandgap (PBG) at optical wavelengths, namely, a high refractive index and a low absorption edge. In general, it is challenging to find materials that fulfill both conditions simultaneously.

## ELECTRODEPOSITION OF $\text{Si}_x\text{Ge}_{1-x}$

In this section, we will focus on the electrodeposition of  $\text{Si}_x\text{Ge}_{1-x}$  as a thin film from two ionic liquids, namely,  $[\text{Py}_{1,4}\text{Tf}_2\text{N}]$  and  $[\text{EMIm}]\text{Tf}_2\text{N}$ . For more information about the electrodeposition of pure Si and pure Ge we refer to refs. [12,14].

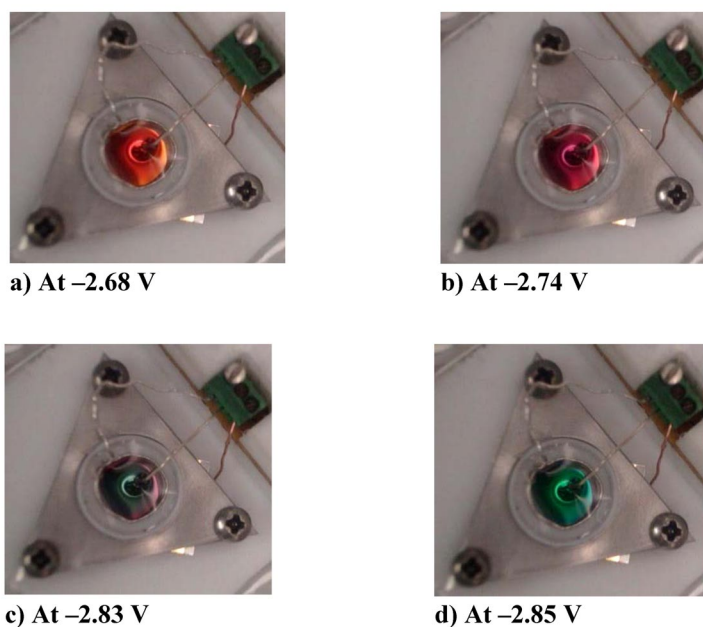
### $\text{Si}_x\text{Ge}_{1-x}$ from $[\text{Py}_{1,4}\text{Tf}_2\text{N}]$

Figure 1 shows the cyclic voltammogram (CV) of an equimolar solution (0.1 M) of  $\text{SiCl}_4$  and  $\text{GeCl}_4$  in  $[\text{Py}_{1,4}\text{Tf}_2\text{N}]$  on Au(111): The first small reduction peak at  $-1$  V might be attributed to the under-potential deposition (UPD) of Ge or the formation of solution species. The second reduction peak at  $-1.7$  V is correlated with the reduction of Ge(IV) to Ge(II), as no deposition at all was visually observed on the Au surface. The third one at  $-2.6$  V is mainly due to the reduction of Ge(II) to Ge(0) likely with some under potential deposition of Si on Ge, since a potentiostatic deposition experiment at this peak potential gives a Ge-rich deposit with quite a small amount of Si. The shoulder at  $-2.9$  V is clearly attributed to the bulk co-deposition of  $\text{Si}_x\text{Ge}_{1-x}$ . The rising current at  $-3.3$  V is corresponding to the irreversible reduction of the organic cation.



**Fig. 1** CV of  $\text{SiCl}_4:\text{GeCl}_4$  (1:1 molar ratio) in  $[\text{Py}_{1,4}]\text{Tf}_2\text{N}$  on Au(111) acquired at a scan rate of 10 mV/s, at 25 °C (see [12]).

Quite an interesting effect was observed during electrodeposition: the deposit showed different strong colors (Fig. 2) ranging from red to blue and finally to green during the running CV in the range from about  $-2.62$  to  $-2.86$  V in the forward scan [12]. Interestingly, the colors disappear and the same color sequence was repeated again in the forward scan from about  $-3.0$  to  $-3.31$  V.



**Fig. 2** Photographs of the electrochemical cell showing the different colors of in situ electrochemically made  $\text{Si}_x\text{Ge}_{1-x}$  in  $[\text{Py}_{1,4}]\text{Tf}_2\text{N}$ . Scan rate = 10 mV/s,  $[\text{SiCl}_4] = 0.1$  M,  $[\text{GeCl}_4] = 0.1$  M, 25 °C (see [12]).

These very interesting colors at room temperature must be due to quantum confinement effects induced by the nanostructure of the deposit, since the red, green, and blue colors indicate that our compound semiconductor  $\text{Si}_x\text{Ge}_{1-x}$  has surely a bandgap between 1.5 and 3.2 eV. In contrast, the bandgap of microcrystalline  $\text{Si}_x\text{Ge}_{1-x}$  ranges from 0.67 eV (for pure Ge) to 1.1 eV (for pure Si) at room temperature, depending on the composition of both elements. Both Ge and Si are indirect semiconductors in the bulk phase, and at room temperature it is very difficult to quench the nonradiative phonon-mediated pathways of electron-hole recombination associated with indirect bandgap semiconductors. However, lattice strain induced by the nanosize of  $\text{Si}_x\text{Ge}_{1-x}$  can transform the lowest inter-band transitions to induce direct bandgap behavior [16,17]. Amorphous semiconductors can also show direct bandgap behavior. The strength of the color is a strong hint for a direct bandgap behavior of our electrochemically made  $\text{Si}_x\text{Ge}_{1-x}$ .

The potentiostatic deposition at  $-2.9$  V leads also to a deposit with more or less the same sequence of colors, which starts to appear after about 30 s of applying the potential. The high-resolution scanning electron microscopy (HR-SEM) picture of the green deposit (Fig. 3) showed a very thin layer (less than 100 nm) with some spherical particles with sizes ranging from 5 to 40 nm on the surface.

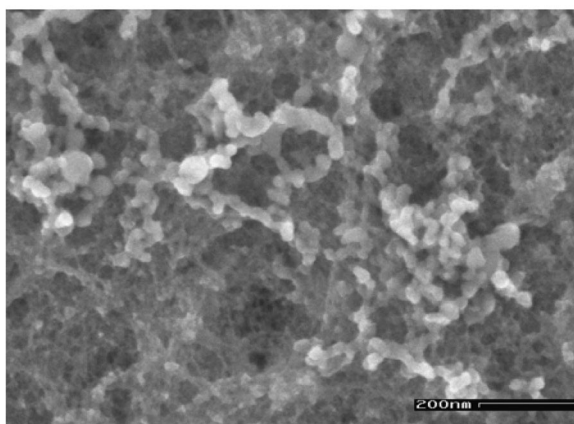


**Fig. 3** HR-SEM image of  $\text{Si}_x\text{Ge}_{1-x}$  after 90 s of the potentiostatic polarization at  $-2.9$  V vs. Ag, where the green color appeared (see [12]).

The energy-dispersive X-ray (EDX) analysis showed that the  $\text{Si}_x\text{Ge}_{1-x}$  deposit made under the described conditions contains both Si and Ge with an overall value of  $\sim 1:1$  with some oxygen due to surface oxidation under ex situ conditions.

As a first approach, the colors can be explained based on light absorption since no photoemission in the dark was observed: With reducing the potential in the CV scan, the deposit gets orange, red, violet, blue, and finally green. The colors must be the result of light absorption, i.e., the deposit absorbs light from 3.2 to 1.5 eV. It is possible and likely that the deposit absorbs light in the near UV and the near IR regime, too. Quantum confinement predicts that the bandgap of a semiconductor increases when the particle size ( $d$ ) is decreased [18]:

$$E_{\text{gap}}(d) = E_{\text{gap}}(\text{bulk}) + c_1/d^2 - c_2/d - c E_{\text{Ry}}$$

$E_{\text{Ry}}$  is the Rydberg energy.  $c_1$ ,  $c_2$ , and  $c$  are constants.

The particles grow with time ( $t$ ), and due to the growth the bandgap is decreased, leading to an overall color change from red to blue–green. The absorbed colors are thus due to particles with different sizes absorbing different wavelengths from the visible spectrum at the same time. Keep in mind that some colors might be a mixture of two or more of other colors. With continuous growth, the particles

become larger and the bandgap becomes smaller to reach that of the bulk material where a rather indirect bandgap behavior arises and no absorption of light occurs due to the small thickness. The growth of new particles on the top of it gives the color sequence again. This might explain why the deposit becomes colorless after a few minutes with repetition of the observed color sequence. We have to point out this is a possible explanation for the observed phenomena. Future studies would involve spectroelectrochemical measurements as well as in situ STM/STS (scanning tunneling spectroscopy), quartz crystal microbalance experiments, and WAXS (wide-angle X-ray spectroscopy). Pulsed potentiostatic electrodeposition might also be helpful to make uniformly sized  $\text{Si}_x\text{Ge}_{1-x}$  nanoparticles.

### $\text{Si}_x\text{Ge}_{1-x}$ from [EMIm] $\text{Tf}_2\text{N}$

From our experience,  $[\text{Py}_{1,4}]\text{Tf}_2\text{N}$  often leads to the electrodeposition of nanomaterials, whereas from  $[\text{EMIm}]\text{Tf}_2\text{N}$  rather microcrystalline deposits are obtained. This has, in our opinion, to do with solvation layers. It was therefore of interest to check if colored  $\text{Si}_x\text{Ge}_{1-x}$  deposits can also be obtained from  $[\text{EMIm}]\text{Tf}_2\text{N}$ . This liquid has the advantage of being less viscous than  $[\text{Py}_{1,4}]\text{Tf}_2\text{N}$  (about 2 times lower [19]), however, at the same time has a lower cathodic decomposition potential. It is stable enough to allow the deposition of  $\text{Si}_x\text{Ge}_{1-x}$  as shown in the CV of an equimolar (0.1 M) solution of  $\text{SiCl}_4$  and  $\text{GeCl}_4$  in  $[\text{EMIm}]\text{Tf}_2\text{N}$  on Au(111) electrode (Fig. 4), which is quite similar to that in  $[\text{Py}_{1,4}]\text{Tf}_2\text{N}$  (Fig. 1) [14].

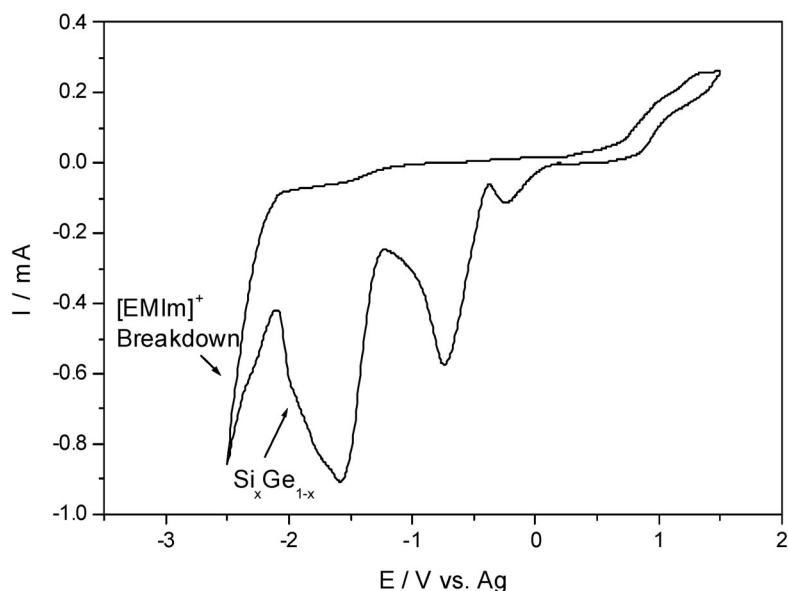


**Fig. 4** CV of  $\text{SiCl}_4:\text{GeCl}_4$  (1:1 molar ratio) in  $[\text{EMIm}]\text{Tf}_2\text{N}$  on Au(111) acquired at a scan rate of 10 mV/s, at 25 °C (see [14]).

Interestingly, the deposit showed, as in  $[\text{Py}_{1,4}]\text{Tf}_2\text{N}$ , a color change (Fig. 5) during the forward scan at the potential of the bulk co-deposition of  $\text{Si}_x\text{Ge}_{1-x}$  ( $E \leq -1.6$  V), indicating an alloy deposition with obvious quantum size effects presumably caused by the nanosize of the deposit. The sequence of the colors, which starts from red, violet, to green, was (as in  $[\text{Py}_{1,4}]\text{Tf}_2\text{N}$ ) repeated during the forward scan. In  $[\text{Py}_{1,4}]\text{Tf}_2\text{N}$ , however, a wider range of  $\text{Si}_x\text{Ge}_{1-x}$  colors was observed and they were stronger in appearance (compare Fig. 5 with Fig. 2). This might be explained by the fact that the deposition rate of  $\text{Si}_x\text{Ge}_{1-x}$  in  $[\text{EMIm}]\text{Tf}_2\text{N}$ , and hence the particle growth that is responsible for the appearance of dif-

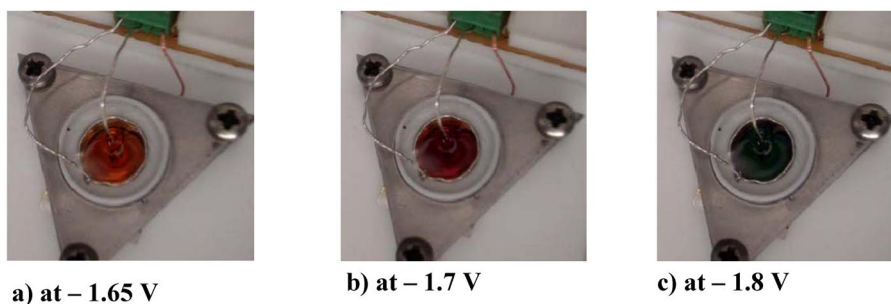


**Fig. 5** Photographs of the electrochemical cell showing the different colors of in situ electrochemically made  $\text{Si}_x\text{Ge}_{1-x}$  in [EMIm]Tf<sub>2</sub>N during the running CV in the forward scan at room temperature. Scan rate = 10 mV/s, [SiCl<sub>4</sub>] = 0.1 M, [GeCl<sub>4</sub>] = 0.1 M (see [14]).

ferent colors, is faster than that one in [Py<sub>1,4</sub>]Tf<sub>2</sub>N. This can be clearly seen from the significantly larger current that flows in [EMIm]Tf<sub>2</sub>N compared with that in [Py<sub>1,4</sub>]Tf<sub>2</sub>N (a factor of ~2) in the same electrochemical cell and at the same solution concentration and reaction conditions. The reason behind this difference in deposition rates might be simple: [EMIm]Tf<sub>2</sub>N has a lower viscosity and as a consequence a higher diffusion rate of electro-active species than in [Py<sub>1,4</sub>]Tf<sub>2</sub>N is achieved. In addition, a possible effect of solvation layers at interfaces, which have an effect on the electrodeposition process, has to be considered. Such solvation layers depend on the liquid and most likely influence electrochemical reactions [20–22].

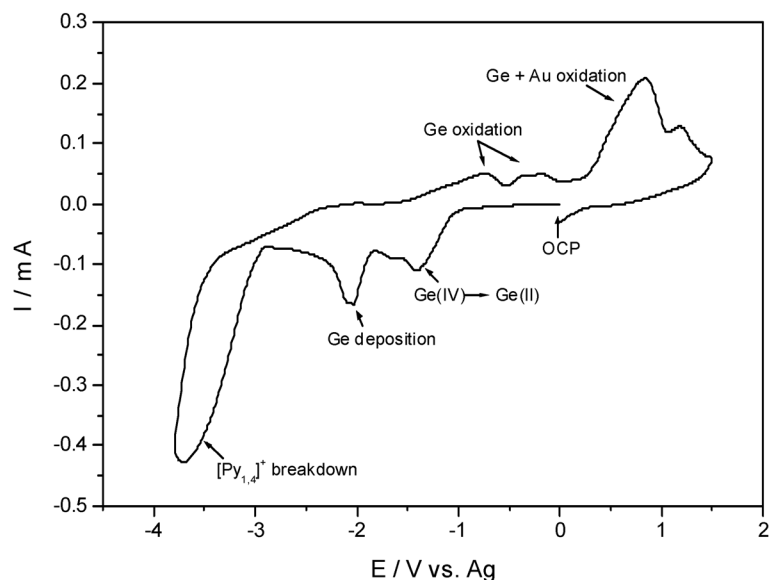
The EDX analysis of the  $\text{Si}_x\text{Ge}_{1-x}$  deposit obtained from [EMIm]Tf<sub>2</sub>N after applying a constant potential of –1.9 V for 1 h, showed clearly a lower Si content than that obtained from [Py<sub>1,4</sub>]Tf<sub>2</sub>N at the same conditions (about 1–1.5:1 overall Si/Ge ratio from [Py<sub>1,4</sub>]Tf<sub>2</sub>N vs. about 1:3 from [EMIm]Tf<sub>2</sub>N). This might also be a reason for the difference in the deposit's colors made in the two different ionic liquids.

## ELECTRODEPOSITION OF Si, Ge, AND OF $\text{Si}_x\text{Ge}_{1-x}$ NANOWIRES

The electrodeposition of the semiconductor nanowires was performed by utilizing track-etched PC membranes (as templates) with an average nominal pore diameter of 90 nm and a thickness and pore density of 16–21  $\mu\text{m}$  and  $10^9 \text{ cm}^{-2}$ , respectively. One side of the membranes was sputtered with roughly 200-nm-thick Au to serve as the working electrode. Dichloromethane was used to dissolve the membrane after deposition in order to get the free nanowires.

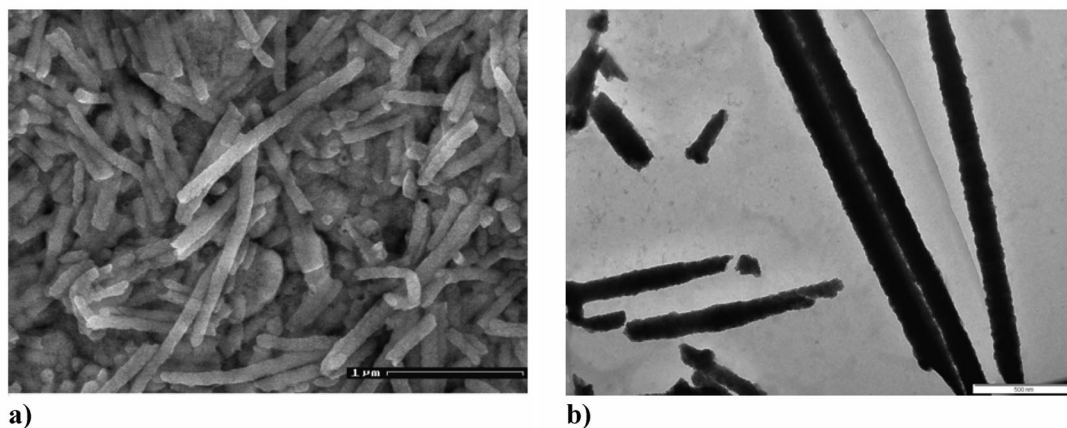
### Ge nanowires

The electrochemical behavior of 0.1 M GeCl<sub>4</sub> in [Py<sub>1,4</sub>]Tf<sub>2</sub>N inside the PC membrane is quite similar to that of a bare Au electrode [12,13] as shown in Fig. 6: The first reduction peak at –1.4 V vs. Ag quasi-reference electrode is correlated with the reduction of Ge(IV) to Ge(II). The shoulder at –1.65 V was not observed in the case of Ge electrodeposition on a bare Au electrode and might be due to transport limitations in the membrane. At –1.86 V, the bulk deposition of Ge takes place and the rising current at –2.9 V corresponds to the decomposition of the organic cation. The oxidation peaks in the back scan are attributed to Ge and Au oxidation, respectively. Due to their usually low surface tension (20–50 mN/m), ionic liquids wet even polymers well, thus facilitating homogeneous electrodeposition inside the membrane.



**Fig. 6** CV of 0.1 M  $\text{GeCl}_4$  in  $[\text{Py}_{1,4}]\text{Tf}_2\text{N}$  inside the PC membrane with an Au-sputtered film on one side of the membrane as a working electrode. Scan rate: 10 mV/s, at 25 °C (see [13]).

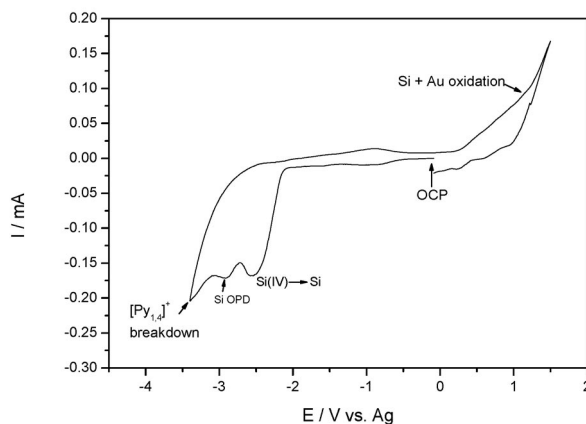
Ge nanowires (Fig. 7a) with a length of about 2  $\mu\text{m}$  and an average diameter of  $\sim 100$  nm were easily obtained after applying a potential of  $-2.1$  V for 1 h. The transmission electron microscopy (TEM) measurements (Fig. 7b) showed that the nanowires have a rough surface, which is mainly controlled by the original shape of the pores of the PC membrane. They are amorphous since no ordered electron diffraction patterns of the nanowires were obtained. EDX analysis of the nanowires [13] showed, besides Ge, small amounts of O due to the ex situ treatment.



**Fig. 7** SEM image (a) and TEM image (b) of Ge nanowires after the dissolution of the PC membrane (see [13]).

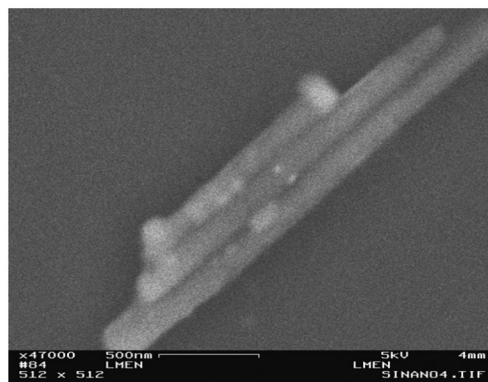
### Si nanowires

Figure 8 shows the CV of 0.5 M SiCl<sub>4</sub> (in [Py<sub>1,4</sub>]Tf<sub>2</sub>N) inside the PC membrane acquired at a scan rate of 10 mV/s at 25 °C. Two main reduction peaks appear in the forward scan: The first one at -2.5 V vs. Ag quasi-reference is due to the bulk deposition of Si. Deposition at -2.5 V on Au(111) without the membrane clearly gives a Si deposit [12]. The second reduction peak at -2.9 V was not observed in the case of 0.1 M SiCl<sub>4</sub> in [Py<sub>1,4</sub>]Tf<sub>2</sub>N, thus it is concentration-dependent and can be attributed further to the over-potential deposition (OPD) of Si. The rising current at -3.1 V is correlated with the decomposition of the organic cation.



**Fig. 8** CV of 0.5 M SiCl<sub>4</sub> in [Py<sub>1,4</sub>]Tf<sub>2</sub>N inside the PC membrane with an Au-sputtered film on one side of the membrane as a working electrode. Scan rate: 10 mV/s, at 25 °C (see [13]).

Figure 9 represents an SEM image of Si nanowires obtained after polarization at -2.8 V vs. Ag quasi-reference electrode for 1 h in the PC membranes. The average diameter of the Si wires is around 100 nm, and the length is more than 3 μm.



**Fig. 9** SEM image of Si nanowires after the dissolution of the PC membrane (see [13]).

### Si<sub>x</sub>Ge<sub>1-x</sub> nanowires

We reported recently, for the first time, our results on the electrodeposition of Si<sub>x</sub>Ge<sub>1-x</sub> nanowires [14]. An equimolar (0.1 M) solution of SiCl<sub>4</sub> and GeCl<sub>4</sub> in [Py<sub>1,4</sub>]Tf<sub>2</sub>N was used for this purpose, which

showed (in the PC membrane) quite a similar electrochemical behavior as on a bare Au electrode.  $\text{Si}_x\text{Ge}_{1-x}$  nanowires were deposited potentiostatically at room temperature. Figure 10 shows an SEM image of  $\text{Si}_x\text{Ge}_{1-x}$  nanowires obtained after polarization at  $-2.2$  V vs. Ag quasi-reference electrode for 1 h. The nanowires have a smooth morphology as shown in the inset figure with an average diameter of  $\sim 100$  nm and a maximum length of approximately  $1 \mu\text{m}$ . The EDX analysis (not shown) of the nanowires showed a Si/Ge ratio of  $\sim 1.5:1$ . The obtained  $\text{Si}_x\text{Ge}_{1-x}$  nanowires are considerably shorter than the previously reported Ge and Si nanowires, provided the same solute concentrations and reaction conditions were applied. This indicates that the deposition of Si alone and of Ge alone is faster than that of the co-deposition of both.

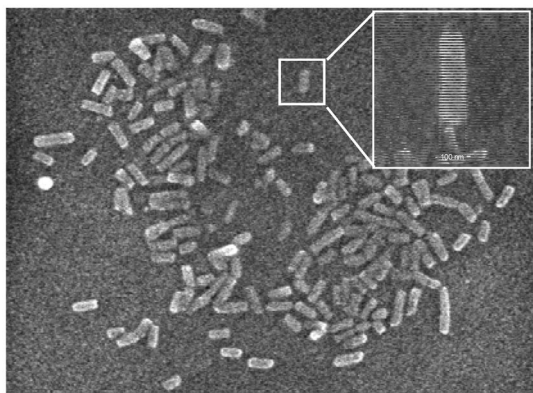


**Fig. 10** SEM image of  $\text{Si}_x\text{Ge}_{1-x}$  nanowires deposited from  $[\text{Py}_{1,4}]\text{Tf}_2\text{N}$  ionic liquid containing equal concentrations (0.1 M) of  $\text{SiCl}_4$  and  $\text{GeCl}_4$  after applying a potential of  $-2.2$  V for 1 h (see [14]).

The aspect ratio of the  $\text{Si}_x\text{Ge}_{1-x}$  nanowires was significantly improved by using the ionic liquid  $[\text{EMIm}]\text{Tf}_2\text{N}$ , which has a viscosity about two times lower than that of  $[\text{Py}_{1,4}]\text{Tf}_2\text{N}$ , and hence higher conductivity and faster deposition rate.

Figure 11 shows  $\text{Si}_x\text{Ge}_{1-x}$  nanowires electrodeposited from an equimolar (0.1 M) solution of  $\text{SiCl}_4$  and  $\text{GeCl}_4$  in  $[\text{EMIm}]\text{Tf}_2\text{N}$  inside the PC membrane (pore diameter = 90 nm), which exhibits a similar electrochemical behavior as in  $[\text{Py}_{1,4}]\text{Tf}_2\text{N}$ .

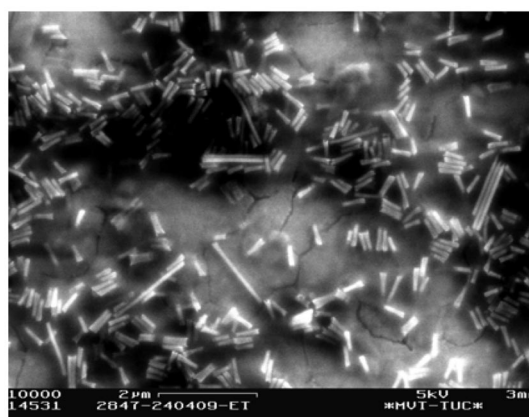


**Fig. 11** SEM image of  $\text{Si}_x\text{Ge}_{1-x}$  nanowires deposited from  $[\text{EMIm}]\text{Tf}_2\text{N}$  ionic liquid containing equal concentrations (0.1 M) of  $\text{SiCl}_4$  and  $\text{GeCl}_4$  after applying a potential of  $-2.2$  V for 30 min (see [14]).

These nanowires were obtained after a polarization at  $-2.2$  V for only 30 min. If we compare them with those obtained from  $[\text{Py}_{1,4}]\text{Tf}_2\text{N}$  (Fig. 10), we can see that they have a maximum length of more than  $2\ \mu\text{m}$ , although just half of the time was applied in the case of  $[\text{EMIm}]\text{Tf}_2\text{N}$ . EDX analysis of the nanowires showed Ge-rich  $\text{Si}_x\text{Ge}_{1-x}$  nanowires with Si/Ge overall ratio of  $\sim 1:3$ . It is quite interesting that the length and the composition of the  $\text{Si}_x\text{Ge}_{1-x}$  nanowires can be varied by simply changing the ionic liquid.

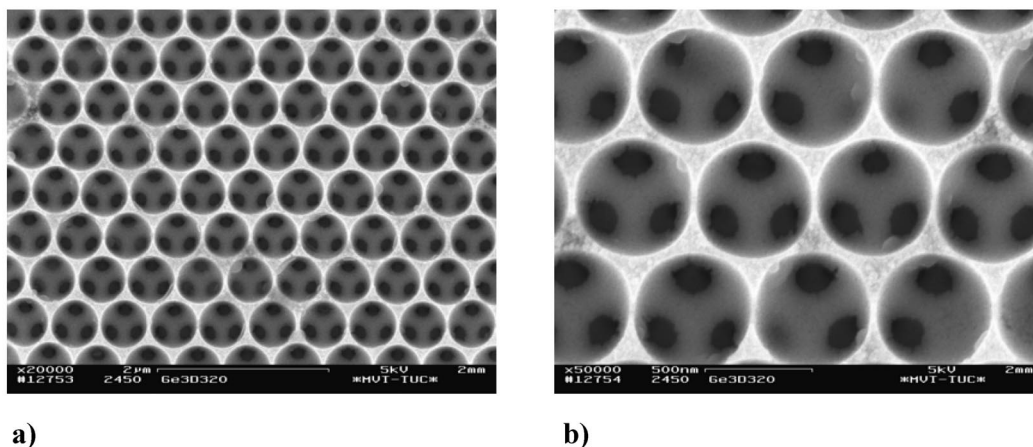
We plan to perform the electrodeposition of semiconductor nanowires from ionic liquids inside PC membranes with pore diameters down to 10 nm. Especially in the case of  $\text{Si}_x\text{Ge}_{1-x}$ , it is interesting to make nanowires in the quantum-confinement size regime.

## ELECTRODEPOSITION OF Ge AND OF $\text{Si}_x\text{Ge}_{1-x}$ PHOTONIC CRYSTALS

### Ge photonic crystals

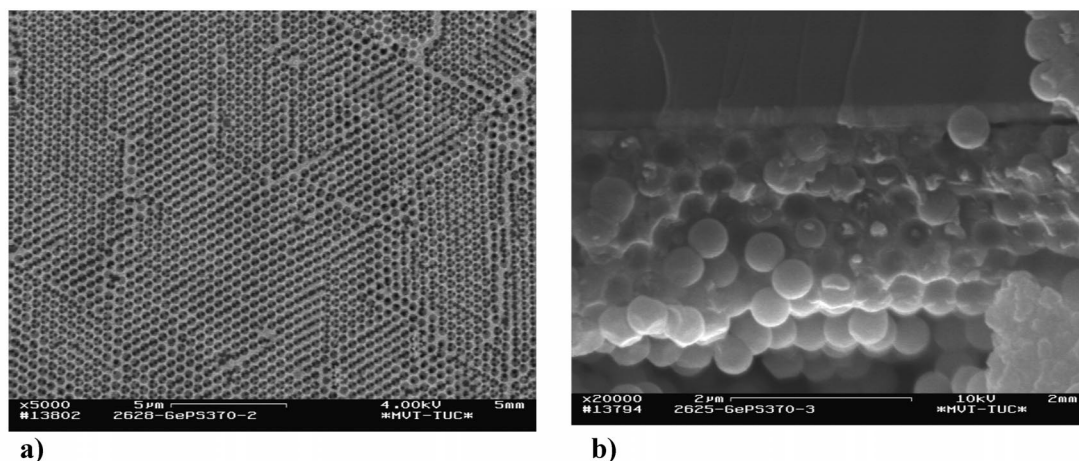
3DOM Ge, which is a prototype of a photonic crystal, was successfully and reproducibly obtained via electrodeposition from 0.1 M  $\text{GeCl}_4$  inside PS colloidal crystal templates with sphere diameter of 560 and 370 nm, respectively. Two ionic liquids were used for this purpose: 1-hexyl-3-methylimidazolium tris(pentafluoroethyl)trifluorophosphate ( $[\text{HMIm}]\text{FAP}$ ) and  $[\text{EMIm}]\text{Tf}_2\text{N}$ . Indium tin oxide (ITO) glass (covered with the PS template) was used as the working electrode [15].

Figure 12a shows an SEM image of a 3DOM Ge layer (after removal of the PS spheres with tetrahydrofuran, THF) deposited from  $[\text{HMIm}]\text{FAP}$  inside the PS template with an average pore diameter of 560 nm. The thickness of this layer is  $1.5\ \mu\text{m}$  obtained after applying a constant electrode potential of  $-1.9$  V vs. Ag quasi-reference electrode for 3 h at room temperature. The deposited Ge has a well-ordered macroporous nanoarchitecture consisting of uniform close-packed spherical pores. The holes into the layer below are clearly visible, indicating the 3-dimensional ordering of the structure. The average center-to-center distance between the pores is measured to be  $555 \pm 10$  nm, indicating that no shrinkage occurs by using the electrodeposition method. The smooth surface morphology in Fig. 12b shows clearly that Ge grows uniformly into the interstices of PS colloidal crystal template.



**Fig. 12** HR-SEM images of 3DOM Ge obtained after applying a constant potential of  $-1.9$  V vs. Ag for 3 h at room temperature (see [15]).

The thickness of 3DOM Ge was improved by using  $[\text{EMIm}]\text{Tf}_2\text{N}$  instead of  $[\text{HMIm}]\text{FAP}$ , and the pore diameter was reduced by using a PS template with sphere diameter of 370 nm, with keeping the other parameters constant. Figure 13a shows an SEM picture of 3DOM Ge obtained from the mentioned



**Fig. 13** (a) SEM image of 3DOM Ge (after removing the PS matrix) obtained after applying a constant potential of  $-2$  V vs. Ag electrode for 30 min (pore size  $\sim 370$  nm). (b) A cross-section of the same sample before the dissolution of the PS spheres (see [15]).

system after applying a constant potential of  $-2$  V vs. Ag quasi-reference for only 30 min. The uniform 3D macroporous structure is clearly observed over a wide area. The obtained 3DOM Ge has a thickness of at least  $2\ \mu\text{m}$  as shown in the cross-sectional SEM image of the sample (before the dissolution of PS template), Fig. 13b.

Figure 14 shows photographs of a whole sample of 3DOM Ge, which has a surface area of  $0.3\ \text{cm}^2$ , with a wide range of colors (orange, yellow, green, and blue) due to light reflection. The coloration and other optical phenomena at the surface of the 3DOM Ge may readily be explained applying a modification of Bragg's law (eq. 1):

$$n \cdot \lambda_{\text{B}} = 2d \cdot \sqrt{n_{\text{eff}}^2 - \sin^2 \theta} \quad (1)$$

Here,  $n$  is the order of the reflection,  $\lambda$  is the wavelength of the PBG, and  $d$  is the lattice plane spacing and  $\theta$  is the angle of incidence to the layer or crystal normal.  $n_{\text{eff}}$  designates an effective index of refraction, usually obtained as (eq. 2):

$$n_{\text{eff}} = f_{\text{fcc}} \cdot n_1 + (1 - f_{\text{fcc}}) \cdot n_2 \quad (2)$$

$n_1$  and  $n_2$  refer to the indices of refraction of air and the material under consideration (1 and 4, respectively, for inverse 3DOM Ge), while  $f_{\text{fcc}}$  is the filling factor for a face-centered cubic arrangement (0.74).

The unusual photonic properties of the inverse Ge opal became manifest on inspection with the bare eye already: on shining a white LED onto the sample, an intense coloration appeared (Fig. 14) which could only be observed if the viewing direction is parallel to the beam originating from the LED (i.e., back-reflection to the left of the normal of incidence, see also Fig. 15). Slight changes of the angle of incidence, by tilting the opal sample, yielded corresponding color shifts. In contrast, a reflection of only low intensity was observed in opposite direction (i.e., light source and viewer on opposing sides of the normal of the interface). Spectra of the 3DOM Ge were obtained using a 450 W Xe lamp coupled to a bifurcated fiber (source and detection are both on the left side of the normal), the exit of which led to an Ocean Optics HR 4000 spectrometer; sample and fiber were mounted on an automatic goniometer. An Al mirror was used as the reflection reference in these measurements, the back-reflected intensities are therefore qualitative only. Reflection measurements on the right-hand side of the normal

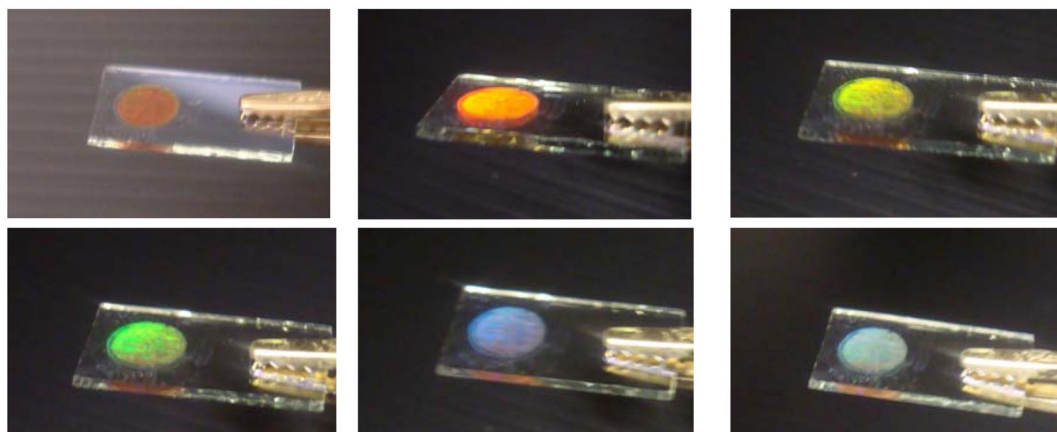


**Fig. 14** Photographs of the deposited Ge photonic crystal (pore size ~370 nm) on ITO-glass substrate showing a color change with changing the angle of the incident visible white light. The deposit was obtained after potentiostatic polarization at  $-2$  V for 30 min in [EMIm]Tf<sub>2</sub>N (see [15]).

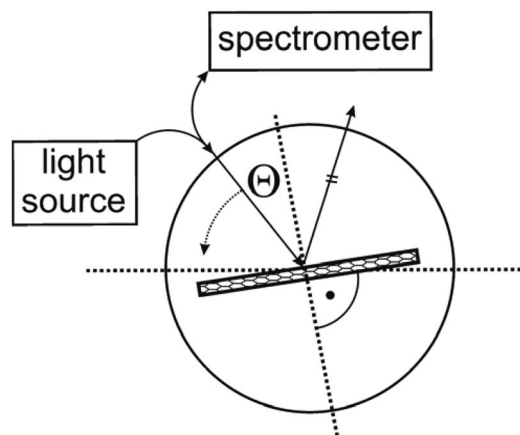


**Fig. 15** Principle measurement set-up used. The marked arrow indicates the direction relative to the normal, for which the 3DOM Ge sample yielded very weak reflection only.

((220) and  $(-220)$  reflections, see below) were calibrated vs. an ITO glass. For comparison, the spectra of an inverse SiO<sub>2</sub> photonic crystal were measured conventionally against a BaSO<sub>4</sub> white standard (i.e., light source and detection on opposite sides of the normal, using two fibers). Figure 16 shows the normalized reflection spectra of the 3DOM Ge sample (average pore size = 370 nm) at different angles of incidence of the irradiating light beam. As suspected from the visual inspection, the optical response of the 3DOM Ge was strongest on the left-hand side of the normal of incidence, while comparably weak signals were found on the right-hand side in the angular regime  $10^\circ < \Theta < 55^\circ$ . The reflections on the left side were allocated in a spectral range between approximately 390 and 670 nm for angles of incidence between  $30^\circ$  and  $64^\circ$ . They characteristically behaved like reflections of a Bragg grating. Experimentally, the observed angular dependence of the reflected wavelength  $\lambda_B$  was found to follow eq. 3.

$$\lambda_B = d \cdot \sin \Theta \cdot \left( \frac{n_1 + n_2}{2} \right) \quad (3)$$

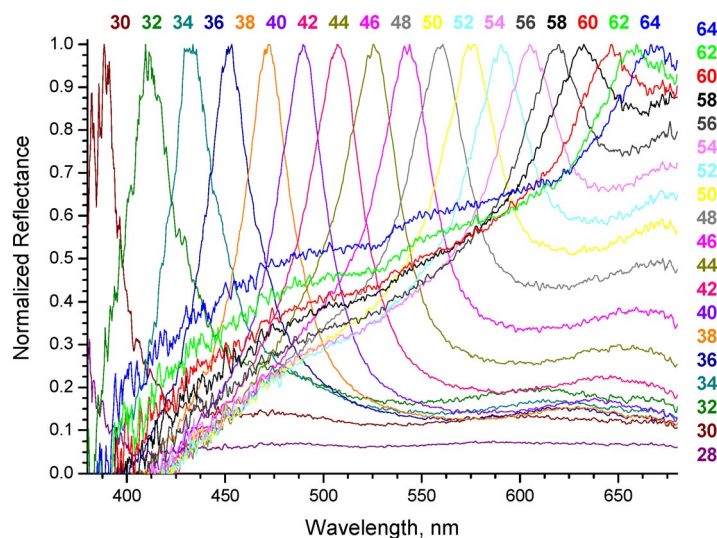


**Fig. 16** Reflectance with a bifurcated fiber at different angles of the 3DOM Ge sample. The numbers in the figure correspond to the angles  $\Theta$  of incidence of the light on the left side of the normal (see also sketch, Fig. 15).

The indices of refraction for air and Ge are denoted  $n_1$  and  $n_2$ , respectively,  $d$  being the distance between (111) planes of the photonic crystal (302 nm for a diameter of 370 nm of the cavities), and  $\theta$  is the angle of incidence. The slight deviation from calculated data (see Fig. 17) may be due to the broad spectral range and reflects the wavelength dependence of the index of refraction. The photonic band resulting in the (111) direction is expected at 1075 nm, as calculated from the lattice spacing and under the assumption of an effective index of refraction of 1.78. Albeit not measured directly, this assumption can be confirmed by monitoring the stop bands arising from the (220) and  $(-220)$  planes of the fcc lattice, both of which are allocated in the visible. They are perpendicular to each other, (220) assuming an

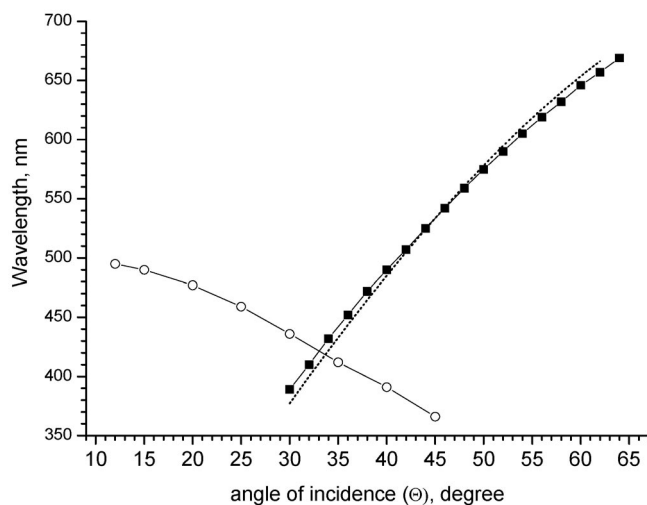


**Fig. 17** Measured (solid squares) and calculated (dotted line) Bragg reflections of the 3DOM Ge sample compared to the stop band evolution of an  $\text{SiO}_2$  inverse opal (open circles). Both inverse opals were prepared from 370 nm spheres.

angle of  $35.3^\circ$  and  $(-220)$  of  $90^\circ$  relative to  $(001)$ . The stop band observed at  $\theta = 35.3^\circ$  then corresponds to perpendicular incidence onto the  $(220)$  plane and appeared at 659 nm. It vanished slowly at angles above  $40^\circ$ , while the gap due to  $(-220)$  started to appear as a shoulder at  $33^\circ$  with steadily increasing intensity to eventually dominate the spectrum. Above  $43^\circ$  the  $(-220)$  stop band is the only distinct feature remaining.

### $\text{Si}_x\text{Ge}_{1-x}$ photonic crystals

Both Si and Ge are very interesting materials for photonic crystals due to their high refractive indices (Ge: 4.12 at  $\lambda = 2000$  nm and Si: 3.53 at  $\lambda = 1100$  nm) and relatively low absorption edges (1870 nm for Ge and 1100 nm for Si, at 300 K) [23]. The previous results on the electrodeposition of  $\text{Si}_x\text{Ge}_{1-x}$  (see above) showed that  $\text{Si}_x\text{Ge}_{1-x}$  with a bandgap of at least 1.5 to 3.2 eV can be obtained. We believe that it would be of great interest to make 3DOM  $\text{Si}_x\text{Ge}_{1-x}$  nanoarchitectures with such bandgap energies (in the quantum size regime). In this case, the absorption edge of the material will be significantly lowered, allowing maybe a complete PBG at “optical wavelengths”.

In this section, we present our first results on the electrochemical synthesis of 2- and 3-DOM  $\text{Si}_x\text{Ge}_{1-x}$ . A solution of  $\text{SiCl}_4:\text{GeCl}_4$  with equal concentrations (0.1 M) in  $[\text{EMIm}]\text{Tf}_2\text{N}$  was used for this purpose. The ionic liquid  $[\text{EMIm}]\text{Tf}_2\text{N}$  was chosen because from our experiments on the electrodeposition of  $\text{Si}_x\text{Ge}_{1-x}$  nanowires and 3DOM Ge, this ionic liquid gives a thicker deposit at a shorter time. Figure 18 shows the CV of this solution (at room temperature) on the ITO substrate covered with a PS template (370 nm average sphere-diameter) which is similar to that on a bare Au electrode (see Fig. 4) but the shoulder of the bulk co-deposition of “SiGe” inside the PS template is broader and clearer. This indicates that the electrodeposition of  $\text{Si}_x\text{Ge}_{1-x}$  inside a template is much slower than that on a bare electrode, which might be attributed to a slower rate of diffusion in a semi-closed area like inside a template compared with an open area of diffusion (a bare surface).

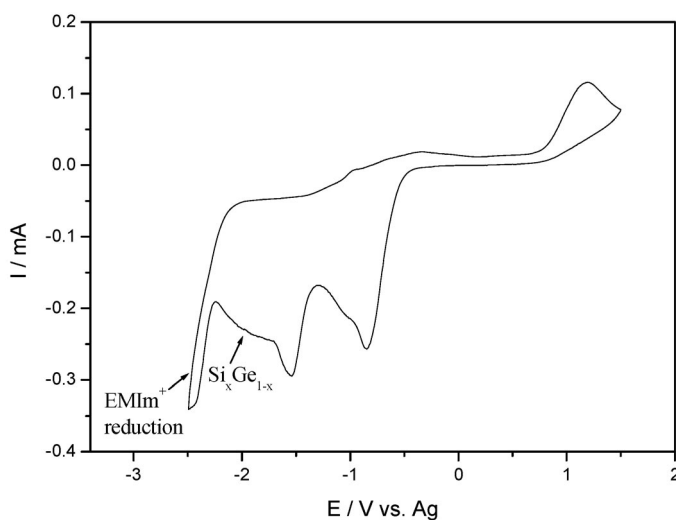


**Fig. 18** CV of  $\text{SiCl}_4:\text{GeCl}_4$  (1:1 molar ratio) in  $[\text{EMIm}]\text{Tf}_2\text{N}$  on the ITO substrate covered with a PS template acquired at a scan rate of 10 mV/s at room temperature.

Figure 19 shows an SEM image of a 2DOM  $\text{Si}_x\text{Ge}_{1-x}$  obtained after polarization at  $-2$  V for 10 min. Although this sample was not 3-dimensional, it showed an angle-dependent reflection when changing the incident angle between it and the artificial white light: the 2DOM  $\text{Si}_x\text{Ge}_{1-x}$  turns red, orange, yellow, green, and blue due to light reflection as seen in Fig. 20.

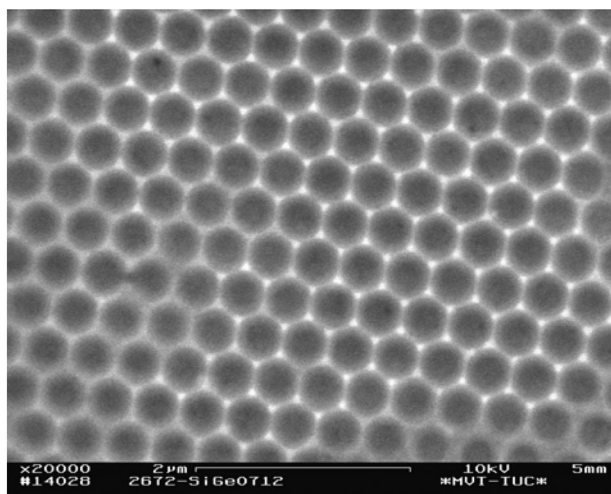


**Fig. 19** SEM image of 2DOM  $\text{Si}_x\text{Ge}_{1-x}$  after the dissolution of the PS template, obtained after a polarization at  $-2$  V for 10 min in a solution of  $\text{SiCl}_4:\text{GeCl}_4$  (1:1) in  $[\text{EMIm}]\text{Tf}_2\text{N}$  at room temperature.

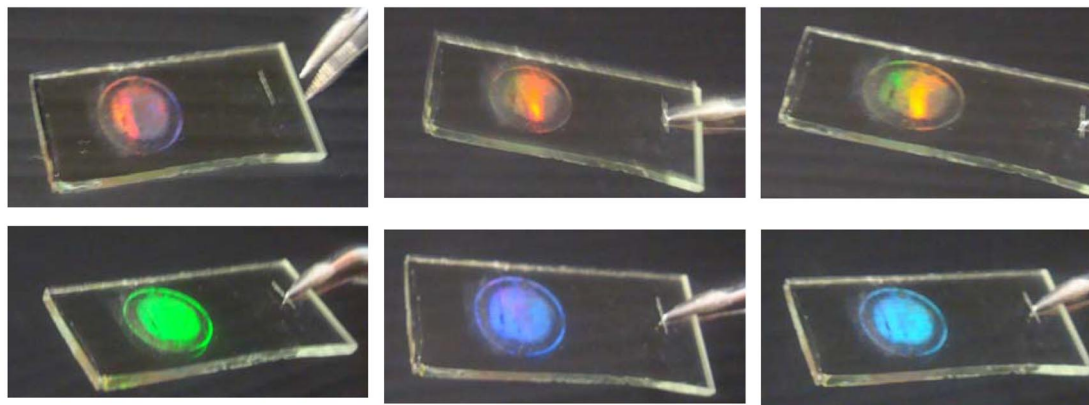


**Fig. 20** Photographs of the deposited 2DOM  $\text{Si}_x\text{Ge}_{1-x}$  photonic crystal (pore size  $\sim 370$  nm) on ITO-glass substrate showing a color change with changing the angle of the incident visible white light. This sample is the same deposit imaged by SEM in Fig. 19.

In order to get 3DOM  $\text{Si}_x\text{Ge}_{1-x}$  the applied deposition time was increased to 30 min. Figure 21 shows the obtained 3DOM  $\text{Si}_x\text{Ge}_{1-x}$  structure. We have to mention here that for the deposition of Ge alone, it is much easier to obtain the 3DOM structure than for  $\text{Si}_x\text{Ge}_{1-x}$  deposition. Moreover, our attempts to make 2DOM or 3DOM Si structures have, hitherto, failed. For unknown reasons, the PS opal structure is disintegrated when Si is deposited.

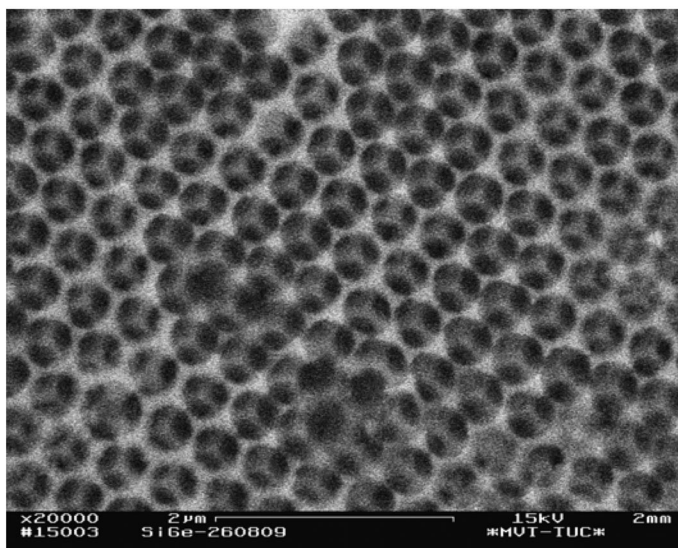


**Fig. 21** SEM image of 3DOM  $\text{Si}_x\text{Ge}_{1-x}$  after the dissolution of the PS template, obtained after a polarization at  $-2$  V for 30 min in a solution of  $\text{SiCl}_4:\text{GeCl}_4$  (1:1) in  $[\text{EMIm}]\text{Tf}_2\text{N}$  at room temperature.

## CONCLUSIONS AND OUTLOOK

From the above results, it can be concluded that electrodeposition from ionic liquids is quite a promising method for the synthesis of high-quality semiconductor nanostructures: the  $\text{Si}_x\text{Ge}_{1-x}$  deposit showed different colors ranging from orange, red, blue, and green, indicating a quantum size effect induced by the nanostructuring of the deposit. Si, Ge, and  $\text{Si}_x\text{Ge}_{1-x}$  nanowires with an average diameter of 90 nm and lengths ranging from 1 to more than 3  $\mu\text{m}$  were easily and reproducibly obtained via electrodeposition inside PC membranes. Highly ordered macroporous Ge and, for the first time,  $\text{Si}_x\text{Ge}_{1-x}$  nanostructures (photonic crystals) were successfully obtained via electrodeposition inside PS colloidal crystal templates with pore sizes of 370 and 560 nm. The complete samples (0.3  $\text{cm}^2$  in area) showed almost all colors of the visible spectrum due to Bragg reflections at different incident light angles. Reflection spectra of our Ge photonic crystal showed clearly that the structure is highly ordered, allowing  $\sim 100\%$  reflectance of different visible-light wavelengths. Our method has many advantages over the traditional ultra-high-vacuum techniques: It is performed at mild conditions, relatively cheap, and the electrodeposition within templates ensures complete infiltration by filling from the bottom up. Future studies will involve: spectro-electrochemical measurements on  $\text{Si}_x\text{Ge}_{1-x}$  deposition, synthesis of semiconductor nanowires with diameters down to 10 nm and applying Ge photonic crystals in the improvement of the efficiency of solar cells.

## REFERENCES

1. T. Trindade, P. O'Brien, N. L. Pickett. *Chem. Mater.* **13**, 3843 (2001).
2. W. Lu, C. M. Lieber. *J. Phys. D: Appl. Phys.* **39**, R387 (2006).
3. O. Leifeld, A. Beyer, E. Müller, D. Grützmacher, K. Kern. *Thin Solid Films* **380**, 176 (2000).
4. R. S. Wagner. *Whisker Technology*, John Wiley, New York (1970).
5. H. J. Fan, P. Werner, M. Zacharias. *Small* **2**, 700 (2006).
6. L. J. Lauhon, M. S. Gudixsen, D. Wang, C. M. Lieber. *Nature* **420**, 57 (2002).
7. K.-K. Lew, L. Pan, E. C. Dickey, J. M. Redwing. *Adv. Mater.* **15**, 2073 (2003).

8. N. D. Zakharov, P. Werner, G. Gerth, L. Schubert, L. Sokolov, U. Gösele. *J. Cryst. Growth* **290**, 6 (2006).
9. A. Izgorodin, O. Winther-Jensen, B. Winther-Jensen, D. R. MacFarlane. *Phys. Chem. Chem. Phys.* **11**, 8532 (2009).
10. F. Endres, D. MacFarlane, A. Abbott. *Electrodeposition from Ionic Liquids*, Wiley-VCH, Weinheim (2008).
11. N. V. Ignat'ev, U. Welz-Biermann, A. Kucheryna, G. Bisssky, H. Willner. *J. Fluorine Chem.* **126**, 1150 (2005).
12. R. Al-Salman, S. Zein El Abedin, F. Endres. *Phys. Chem. Chem. Phys.* **10**, 4650 (2008).
13. R. Al-Salman, J. Mallet, M. Molinari, P. Fricoteaux, F. Martineau, M. Troyon, S. Zein El Abedin, F. Endres. *Phys. Chem. Chem. Phys.* **10**, 6233 (2008).
14. R. Al-Salman, F. Endres. *J. Mater. Chem.* **19**, 7228 (2009).
15. X. Meng, R. Al-Salman, J. Zhao, N. Borisenko, Y. Li, F. Endres. *Angew. Chem., Int. Ed.* **48**, 2703 (2009).
16. Y. S. Tang, S. E. Hicks, C. D. W. Wilkinson, C. M. Sotomayor Torres, W. X. Ni, J. Birch, J. B. Joelsson, G. V. Hansson, A. Kvick, K. L. Wang. *Proc. SPIE* **3007**, 170 (1997).
17. S. Froyen, D. M. Wood, A. Zunger. *Thin Solid Films* **183**, 33 (1989).
18. V. A. Singh, V. Ranjan, M. Kapoor. *Bull. Mater. Sci.* **22**, 563 (1999).
19. H. Tokuda, S. Tsuzuki, M. A. B. H. Susan, K. Hayamizu, M. Watanabe. *J. Phys. Chem. B* **110**, 19593 (2006).
20. M. Mezger, H. Schröder, H. Reichert, S. Schramm, J. S. Okasinski, S. Schöder, V. Honkimäki, M. Deutsch, B. M. Ocko, J. Ralston, M. Rohwerder, M. Stratmann, H. Dosch. *Science* **322**, 424 (2008).
21. R. Atkin, G. G. Warr. *J. Phys. Chem. C* **111**, 5162 (2007).
22. F. Endres, S. Zein El Abedin. *Phys. Chem. Chem. Phys.* **8**, 2101 (2006).
23. D. J. Norris, Y. A. Vlasov. *Adv. Mater.* **13**, 371 (2001).